Food Chemistry: X 27 (2025) 102450

Contents lists available at ScienceDirect

Food Chemistry: X

journal homepage: www.sciencedirect.com/journal/food-chemistry-x

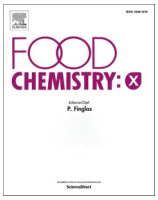

Effect of Ca^{2+} on the structure of collagen fibers in sea cucumber (*Apostichopus japonicus*) under low-temperature tenderization condition

Chen Zhang [b], Wei Wang [b], Hongyan Li [b], Hongxia Che [b], Wancui Xie [b,d], Wenming Ju [d], Hang Qi [c], Xiufang Dong [a,b,*]

[a] School of Public Health, Dali University, Dali, Yunnan 671003, PR China
[b] Shandong Provincial Key Laboratory of Biochemical Engineering, College of Marine Science and Biological Engineering, Qingdao University of Science and Technology, Qingdao, Shandong 266042, PR China
[c] National Engineering Research Center of Seafood, School of Food Science and Technology, Dalian Polytechnic University, Dalian, Liaoning 116034, PR China
[d] Homey Group International Inc., Rongcheng, Shandong 264305, PR China

ARTICLE INFO

Keywords:
Sea cucumber (*Apostichopus japonicus*)
Collagen fibers
Ca^{2+}
Low-temperature tenderization
Structural stability

ABSTRACT

Collagen fibers (CFs) are essential in maintaining the structural integrity of sea cucumber body wall tissues. Addition of Ca^{2+} to meat products improves tenderness and modulates the levels of chemical interactions in CFs. In this study, we investigated the effects of Ca^{2+} (ranging from 0 to 40 mM) on the structural organization and thermal stability of CFs. The dissolution of protein and polysaccharide of sea cucumber collagen fiber was less under low concentration of Ca^{2+} (2.5 mM–10 mM), and the dissolution amount corresponding to high concentration of Ca^{2+} (20 mM, 40 mM) increased. FTIR, XRD, DSC, TGA and SEM analyses revealed that low concentrations of Ca^{2+} (2.5 and 5 mM) increased the intermolecular binding of CFs, enhanced stability of triple helix structure, maintained the structural integrity of CFs, and inhibited the degradation of CFs. This study provides insights into enhancing the quality of sea cucumber through low-temperature tenderization.

1. Introduction

Sea cucumber (*Apostichopus japonicus*) is a member of the phylum Echinodermata and the class Holothuroidea, and is primarily found in Northeast Asia, including China, Korea, and Japan. There are nearly 1400 species of sea cucumbers globally, with more than 40 edible species (Shakouri et al., 2009; Xu et al., 2015). The main edible component of *A. japonicus* is the body wall (AJBW), which is a mutable collagenous tissue (MCT) mainly composed of collagen, proteoglycans and glycoproteins (Thurmond & Trotter, 1996). Collagen molecules are connected at the head and tail, quarter-staggered, and arranged in parallel according to specific rules. Collagen molecules are helically entangled through covalent cross-linking, forming stable collagen fibrils. These fibrils are further assembled into collagen fibers (CFs) through the linkage of proteoglycan bridges (Tian et al., 2020). Consequently, CFs play a significant role in maintaining the structural integrity of the body wall tissue. Low-temperature heating has been applied to the tenderization of beef and pork to improve the eating quality of meat products. Low-temperature tenderization technique is often used to moderately degrade the structural proteins in muscle tissue that maintain the integrity of myofibrillar (Dong, He, et al., 2020). Similarly, in order to obtain the most desirable products, a low-temperature treatment technology can be applied to sea cucumber processing.

Numerous studies demonstrated that addition of Ca^{2+} enhances meat tenderness by activating calcium-activated enzymes and altering the structure and conformation of myofibrillar proteins (Li et al., 2017; Wang et al., 2020). Furthermore, Ca^{2+} affects the degree of bonding between the chemical interaction of CFs. Moreover, Ca^{2+} is significantly associated with the mechanical and structural properties of CFs, enhancing the degree of cross-linking of CFs mainly through the formation of chelating rings by binding to the carboxyl groups in collagen amino acid residues (Pang et al., 2017). Ca^{2+} promotes protein unfolding by inducing protein conformational changes and weakening intramolecular hydrophobic interactions, ultimately exposing hydrophobic amino acid residues and enhancing protein cross-linking (Jia et al., 2015; Wang et al., 2020; Zhou & Yang, 2019). Previous findings indicate that Ca^{2+} concentration has a bidirectional effect: at low concentration (1 mM) Ca^{2+} promotes collagen self assembly, resulting in stabilization of collagen protein structure. Conversely, at higher concentration of Ca^{2+} (14 mM), the degree of collagen self-assembly

* Corresponding author at: School of Public Health, Dali University, Dali, Yunnan 671003, PR China
E-mail address: dxf900321@126.com (X. Dong).

https://doi.org/10.1016/j.fochx.2025.102450
Received 8 May 2024; Received in revised form 19 August 2024; Accepted 7 April 2025
Available online 8 April 2025

decreases, whereas the mineral crystallinity remains optimal (Niu et al., 2017). These findings indicate that Ca^{2+} has a beneficial effect on improving the tenderness of meat products and influencing cross-linking of CFs. However, the mechanism underlying the effect of Ca^{2+} on the structure of CFs is yet to be elucidated.

Collagen fibers are a good model for the study of AJBWs. They are extracted from the AJBW, and both water-soluble and acid-soluble components are removed and they lack endogenous enzymes (Dong et al., 2021). In this study, we evaluated the effect of $CaCl_2$ on dissolution of soluble proteins, polysaccharides, and TCA-soluble oligopeptides in sea cucumber CFs under low-temperature tenderization conditions. In addition, we explored the primary and secondary structural changes using FTIR and XRD techniques and characterized the thermal properties through DSC and TGA analysis. The aim of the study was to elucidate the effects of Ca^{2+} on the structure of CFs and to enhance the theoretical understanding of improving the quality of sea cucumber products.

2. Material and methods

2.1. Materials

Live sea cucumbers (AJ) weighing 70 ± 10 g each were purchased from the Qingdao Kai Ping Road Fish Market (Qingdao, Shandong Province, China), and promptly transported to the laboratory in cold seawater protected from light.

2.2. Preparation of CFs

Collagen fibers were extracted according to a previously described method (Dong, Shen, et al., 2020). Live sea cucumbers were eviscerated, washed with distilled water and weighed. AJBWs were cut into small pieces (5 mm × 5 mm × 1 mm), homogenized and then incubated in distilled water (w:v = 1:5) at 4 °C for 1.5 h. The samples were centrifuged and the precipitates were washed twice with distilled water. Subsequently, the precipitate was mixed with 0.5 M acetic acid (w:v = 1:5) and stirred for 72 h. The mixture was then washed with distilled water to obtain purified CFs as CON group.

2.3. Experimental design

The extracted CFs were mixed with 0, 2.5, 5, 10, 20, 40 mM $CaCl_2$ in the ratio of 1:10 (w:v) and incubated at 37 °C for 12 h to explore the effect of different Ca^{2+} concentrations on the structural characteristics of CFs. The thermal treatment conditions were optimized to achieve the most intense tenderization as described in previous research (Dong et al., 2018). After incubation with different concentrations of $CaCl_2$, the samples were centrifuged at 13,500 ×*g* for 15 min at 4 °C. Subsequently, the precipitate after centrifugation was subjected to dialysis to remove salt and was then lyophilized. The lyophilized powder was reconstituted with the same volume of distilled water to obtain a solution. The intact fragments of CFs and solution were stored for subsequent experiments.

2.4. Assessment of chemical compositional changes in the soluble component of CFs

2.4.1. Chemical analysis

The lyophilized powder sample was reconstituted with distilled water and the soluble protein content of the samples was assessed using the BCA protein assay kit (Epizyme Biotech, Shanghai, China). The amount of soluble polysaccharide was measured using the phenol-sulfuric acid method (DuBois et al., 1956). TCA-soluble oligopeptide content of the samples was evaluated as described in previous studies (Wu et al., 2013; Yang et al., 2015).

2.4.2. Sodium dodecyl sulphate polyacrylamide gel electrophoresis (SDS-PAGE)

SDS-PAGE was conducted to explore the protein patterns using a method described in a previous study (Laemmli, 1970) with 10 % separating and 5 % stacking gels. Samples after reconstitution of lyophilized powder in distilled water were mixed with SDS-PAGE sample buffer containing 5 % β-mercaptoethanol at a ratio of 4:1 and boiled for 5 min. The samples (10 μL) and markers were loaded into wells. Electrophoresis was performed at a constant current of 15 mA for the stacking gel and 30 mA for the separating gel. After electrophoresis, the gels were stained sequentially with 0.05 % Coomassie Brilliant Blue R-250 and 0.5 % Toluidine blue in 0.5 % formic acid.

2.5. Structural changes in intact fragments of CFs

2.5.1. Fourier transform infrared spectroscopy (FTIR)

The freeze-dried intact CFs fragments, both before and after incubation with different Ca^{2+} treatments, were mixed with KBr (1 mg/100 mg) and the structural changes were evaluated using a FTIR (IS50, Thermo Fisher Scientific CO., Waltham, MA, USA). The scanning range was 4000 to 1000 cm^{-1} with 64 scans per sample.

2.5.2. X-ray diffraction (XRD) analysis

The lyophilized samples were cut into small pieces and analyzed using an X-ray diffractometer (SmartlabSE, Rigaku Ltd., Tokyo, Japan) equipped with Cu-Kα radiation. The data was collected in a scanning range of 2θ from 5 to 90° and a scanning speed of 10 °C/min. The d value was calculated using the Bragge' equation (He et al., 2021) as shown below (Eq. (1)):

$$d\ (nm) = \lambda / 2\sin\theta \quad (1)$$

where λ represents the wavelength of the radiation source (λ = 0.15418 nm), and θ denotes the angle of the diffraction peak.

2.5.3. Differential scanning calorimetric (DSC) analysis

Thermal stability analysis of freeze-dried intact CFs fragments before and after incubation with different Ca^{2+} treatments was conducted using differential scanning calorimetry method (DSC1, Mettler toledo, Columbus, OR, USA). The heating temperature ranged from 20 to 80 °C with a steady increase of 1 °C /min and a constant nitrogen flow, according to a previously described method (Song et al., 2022; Yan et al., 2022).

2.5.4. Thermogravimetric (TGA) analysis

TGA analysis was conducted as described in a previous study (Yu et al., 2018). A freeze-dried powder sample weighing 5 mg was transferred into a thermal analyzer (STA4495F5, NETZSCH Ltd., Bavaria, Germany) and heated from 40 to 640 °C at a rate of 10 °C /min under a protective nitrogen atmosphere.

2.5.5. Scanning electron microscopy

The freeze-dried intact CFs fragments, both before and after incubation with different Ca^{2+} treatments were mounted on a metal stub, coated with Pb, and then the images were produced using a S-4800 scanning electron microscopy (HITACHI Ltd., Tokyo, Japan) with the acceleration voltage set at 2 kV(Dong et al., 2020b).

2.6. Statistical analysis

All experiments were performed with at least three replicates. Data are presented as mean ± standard deviation (SD). SPSS 26.0 software (SPSS Inc., Chicago, IL, USA) was used for statistical analysis. Differences between means were assessed using a one-way analysis of variance, followed by S-N-K post hoc test. P values <0.05 indicate statistically significant differences.

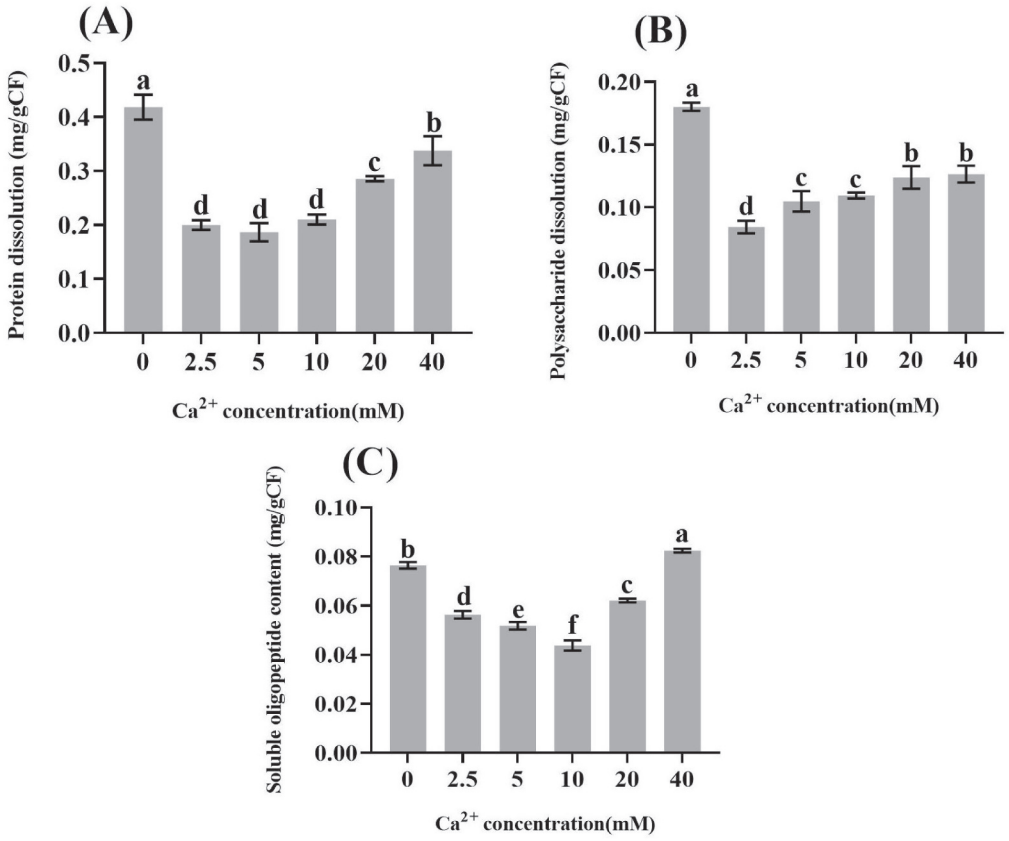

Fig. 1. Changes in proteins (A), polysaccharide (B), soluble oligopeptides (C) of collagen fibers (CFs) dissolution. Values of different groups with different lower-case letters are significantly different at $P < 0.05$.

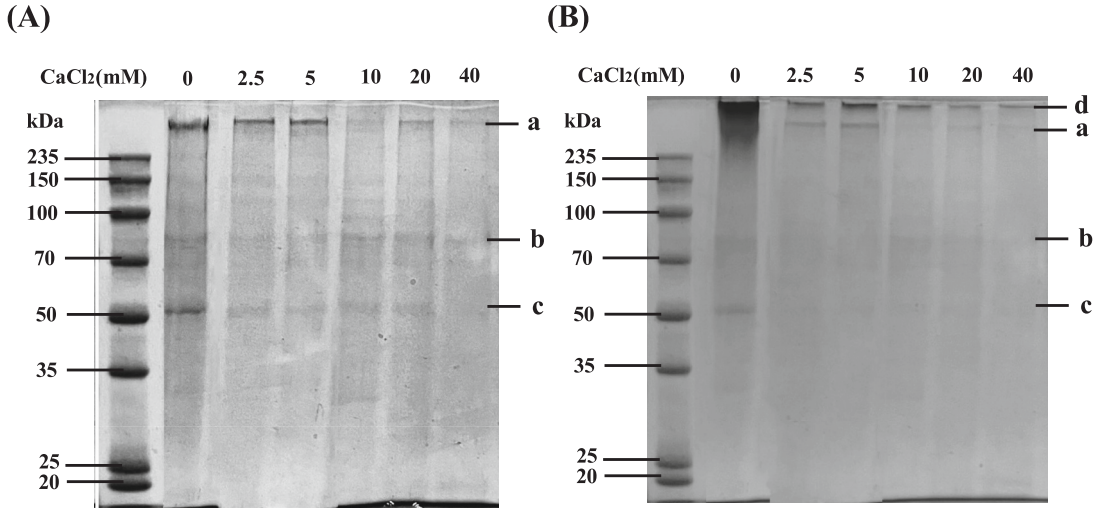

Fig. 2. Ca^{2+}-treated protein distribution pattern of sea cucumber CFs model. (A) Coomassie Brilliant Blue R-250 protein staining; (B) Toluidine blue sugar staining. (For interpretation of the references to colour in this figure legend, the reader is referred to the web version of this article.)

3. Results

3.1. Composition analysis of dissolved content

3.1.1. Changes in soluble components of CFs

The contents of proteins, polysaccharides and TCA-soluble components released from CFs after incubation with different Ca^{2+} concentrations were determined (Fig. 1A-C). The dissolution rates of proteins, polysaccharides and TCA-soluble components in the group that was treated with 0 mM $CaCl_2$ were 0.418 ± 0.023 mg/g CFs, 0.181 ± 0.003 mg/g CFs and 0.764 ± 0.001 mg/g CFs. The contents of proteins, polysaccharide and TCA-soluble component decreased with increased Ca^{2+} concentrations and then increased. Protein solubilization was lowest at 5 mM $CaCl_2$. In contrast, polysaccharide solubilization was minimum at 2.5 mM $CaCl_2$ and TCA-soluble solubilization was lowest at 10 mM $CaCl_2$, which were 0.45-fold, 0.47-fold, and 0.57-fold compared

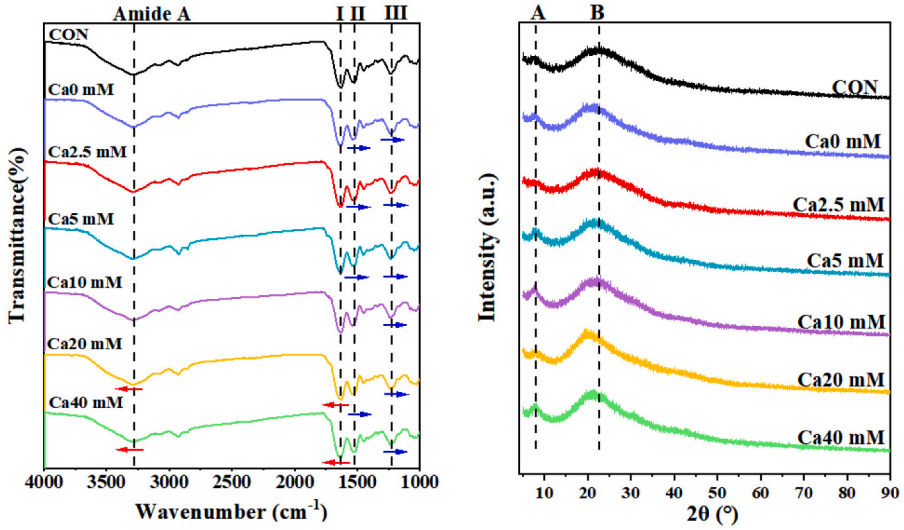

Fig. 3. Microstructure characterization of CFs models for at 37 °C for 12 h. (A) Fourier transform infrared radiation (FTIR) spectra of Ca^{2+} with different concentrations; (B) X-ray diffraction (XRD) diagram of Ca^{2+} with different concentrations.

to the 0 mM group, respectively. However, the protein and polysaccharide solubilization at 40 mM $CaCl_2$ was lower than in the 0 mM group by 0.19-fold and 0.29-fold, respectively. The content of TCA-soluble oligopeptides increased by 1.079-fold after treatment with 40 mM $CaCl_2$ relative to the control. These findings show that Ca^{2+} affected the dissolution of soluble components, therefore, we evaluated the effect of Ca^{2+} treatment on the primary and secondary structure and thermal degradation properties of CFs.

3.1.2. *Effect of Ca^{2+} on the degree of degradation of proteins and polysaccharides in CFs*

SDS-PAGE electrophoresis was performed to determine the relative molecular weight, size and distribution of sulfated polysaccharides and proteins (Li et al., 2024; Liu et al., 2019). The results of staining of proteins using Coomassie Brilliant Blue R-250 are presented in Fig. 2A. Three main bands, a, b, and c, were observed in each group. After the addition of Ca^{2+}, the gray scale of the a and c bands decreased, and the decrease of 40 mM was the most significant. The findings showed that 10 and 20 mM Ca^{2+} gradually degraded macromolecular proteins in collagen to form small peptides. A band observed between the separating gel and 235 kDa represented the most extensively distributed protein region. The bands appeared darkest when Ca^{2+} concentration was 5 mM and became lighter as larger proteins were degraded with 40 mM Ca^{2+} concentration. The treatment with 40 mM resulted in dissolution of protein to predominantly small molecule oligopeptides correlating with the TCA-soluble oligopeptide results (Fig. 1C). Proteolysis involves the degradation of the bridging structure of collagen and the polymerization between collagen fibrils, leading to loss of internal stability of CFs, disappears and the dispersion of collagen fibrils.

The SDS-PAGE electrophoresis results of the dissolved material re-stained with toluidine blue are presented in Fig. 2B. A substantial amount of polysaccharide solubilization in the 0 mM Ca^{2+} group likely resulted in a significant decrease in the stability of CFs during heat treatment. The intensity of band a and d decreased with an increase in Ca^{2+} concentration, whereas band b and c exhibited insignificant change in intensity. The intensity of band d increased at 5 mM and decreased after treatment with 40 mM Ca^{2+}. This finding indicates that the structure of CFs was not significantly damaged at 5 mM Ca^{2+}, as it still existed in the form of proteoglycan. However, the intensity of band d gradually decreased with an increase in Ca^{2+} concentration, indicating that some proteins separated from the polysaccharide molecules, thereby increasing the relative content of small molecular weight polysaccharides (Wang et al., 2020). SDS-PAGE analysis confirmed the observed alterations in soluble components.

3.2. *Microstructure characterization of CFs*

3.2.1. *Fourier transform infrared spectroscopy of CFs treated with different concentrations of Ca^{2+}*

FTIR spectroscopy was conducted to assess further the effect of different Ca^{2+} concentrations on the conformation of proteins within CFs (Fig. 3A). Each sample exhibited four similar characteristic peaks. The peak of amide A, resulting from N—H stretching vibrations, was observed at 3300 cm^{-1}. Amide *I* band, indicated by the stretching vibration of C═O in the protein polypeptide backbone and sensitive to changes in the three-stranded helical structure, exhibited a characteristic absorption peak at 1640 cm^{-1}. The amide II band, arising from C—N stretching vibrations and N—H bending vibrations appeared at 1535 cm^{-1}. The characteristic absorption peak of the amide III band was observed around 1235 cm^{-1}, caused by a combination of C—N stretching vibrations and N—H bending vibrations, sometimes accompanied by a small amount of C—O in-plane bending vibrations and C—C stretching vibrations. Higher peaks of amide bands indicated low structural stability and weakened hydrogen bonds (Li et al., 2024; Thongchai et al., 2020; Zou et al., 2023). The amide A band and amide I band of the samples treated with 20 mM and 40 mM Ca^{2+} exhibited red shifts compared with the CON (Fig. 3A). This phenomenon can be attributed to the formation of hydrogen bonds between the carbonyl group in the three-stranded helical structure of collagen and N—H and O—H on adjacent amino acid chains, and the formation of ligand bonding through the complexation of Ca^{2+} with C═O. These interactions weakened the role of non-covalent bonding and hydrogen bonding. The weakening of the interactions among the three strands of collagen led to an increase in the diameter of the molecules and a reduction in their stability. The amide II and amide III bands of CF exhibited a blue shift after treatment with Ca^{2+} compared with the CON.

3.2.2. *X-ray diffraction of CFs treated with different concentrations of Ca^{2+}*

The spatial structure of collagen, including the three-stranded helical conformation of collagen molecules and the axial arrangement of collagen protofibrils, was determined by X-ray diffraction analysis (Zheng et al., 2022). In the XRD pattern, the peak position indicates the diffraction angle, the peak height represents the diffraction intensity, and the peak width indicates the crystallization level of the substance

Table. 1
Values of θ and d corresponding to the diffraction A-peak of CFs treated with Ca^{2+} of different concentrations.

Ca^{2+} concentrations(mM)	CON	0	2.5	5	10	20	40
2θ(°)	7.74	7.66	7.67	7.68	7.67	7.65	7.64
d value (nm)	1.142	1.154	1.152	1.151	1.152	1.155	1.156

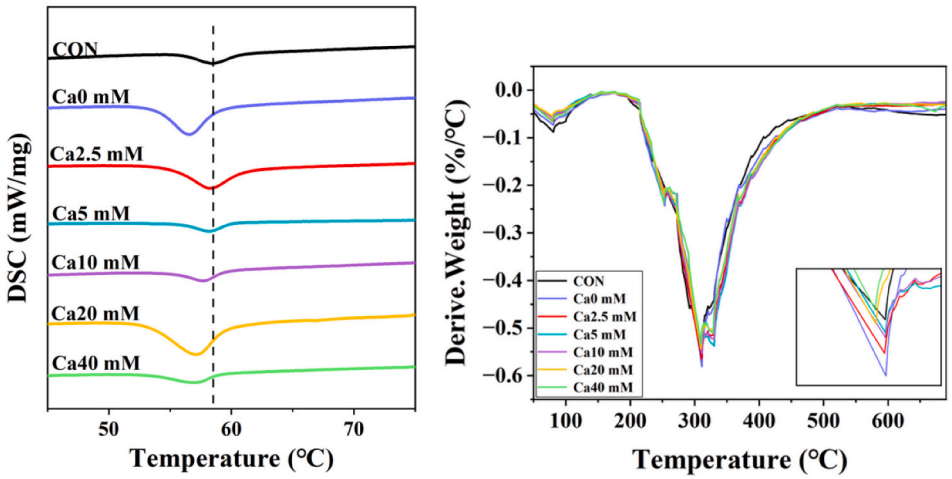

Fig. 4. Thermal stability of CFs models for at 37 °C for 12 h. (A) Differential scanning calorimetry (DSC) of Ca^{2+} with different concentrations; (B) Derivative thermogravimetry (DTG) chart of Ca^{2+} with different concentrations.

(Gao et al., 2020). Each group of samples exhibited two distinct diffraction peaks (Fig. 3B). The first diffraction peak, observed between 7° and 8°, indicated the distance between the molecular chain of CFs and the relatively regular part of the CFs internal structure that generated the diffraction peak. The value of d corresponding to each peak was calculated using Bragg's equation based on the wavelength of the X-rays and the θ angle. The d value of peak A represented the distance between CFs chains and was calculated as shown in Table 1. The d value for the CON group was 1.14 nm, indicating an intact structure of CFs. The increase in d value after heat treatment for 12 h at 37 °C compared with the CON indicated that heat treatment disrupted cross-linking between CFs. Peak a shifted slightly after addition of Ca^{2+}. Peak a shifted to a higher angle in the 2.5 Ca^{2+} and 5 mM Ca^{2+} groups, decreasing the d values by 0.002 nm and 0.003 nm, respectively. The d values of the groups treated with 10, 20 and 40 mM at Ca^{2+} concentrations increased to 1.152, 1.155 and 1.156 nm, respectively, compared with the 0 mM group. Low concentrations of Ca^{2+} reduced the spacing between the molecular chains of CFs and resulted in tighter binding of CFs, whereas high concentrations of Ca^{2+} had the opposite effect. The second peak observed was the amorphous diffraction peak near 22°, characterized by a broader peak shape, representing the diffraction of X-rays by the numerous structural layers within CFs. Peak B in the 20 mM and 40 mM groups gradually shifted towards higher diffraction angles compared with the 0 mM group, whereas this peak shifted towards lower diffraction angles in the 2.5 mM and 5 mM groups. This indicates a specific alteration in the crystallinity of CFs. The third peak, around 31–32°, exhibited a small and broad peak shape, reflecting the spacing between adjacent amino acid residues on the helix center axis in the CF three-stranded helix structure. However, none of the seven groups of samples showed significant diffraction peaks at 31–32°. We hypothesized that only a small fraction of Ca^{2+} penetrates the three-stranded helix structure to alter its microstructure. Instead, the Ca^{2+} potentially aggregate more between the collagen molecular chains and bind with certain groups of collagen, forming a more stable chemical bond to replace the weaker hydrogen bonding and van der Waals forces (Gao et al., 2020).

3.3. Thermal stability analysis of CFs

3.3.1. Differential scanning calorimetry of CFs treated with Ca^{2+} at different concentrations

DSC analysis was conducted to explore variations in CFs primary structure (Ge et al., 2022; Guo et al., 2024). Intact collagen is composed of three polypeptide chains intertwined with each other, and exposure to heat breaks hydrogen bonds, destroying the natural conformation. The lyophilized powder was subjected to DSC analysis after incubation with Ca^{2+}, as shown in Fig. 4A. All samples showed a characteristic absorption peak attributed to the disruption of the helical structure and covalent bonds between collagen molecules caused by the damage of the tertiary structure of collagen (Bu et al., 2020). The lowest peak represented the thermal denaturation temperature (T_{max}) of CFs. The T_{max} of the CON group was 58.41 °C, consistent with previously reported findings (Liu et al., 2017). The T_{max} (56.53 °C) of 0 mM decreased by 1.88 °C compared with the CON group. These findings indicate that heat treatment significantly reduced the stability of CFs. The T_{max} initially exhibited an increasing trend followed by a decrease with an increase in Ca^{2+} concentration. The thermal degradation temperature increased under low concentrations of $CaCl_2$, whereas the T_{max} shifted to the left for the 10 mM, 20 mM, and 40 mM Ca^{2+} groups.

3.3.2. Thermogravimetric analysis of CFs treated with different concentrations of Ca^{2+}

The TGA of CFs following incubation with different concentrations of Ca^{2+} are presented in Fig. 4B. The TGA curve of the CFs exhibited two distinct stages. The first stage extended from room temperature to approximately 170 °C. This stage was characterized by loss of mass, which was mainly attributed to the evaporation of adsorbed water and small molecules (Liu et al., 2016). The maximum weight loss rate for the groups treated with Ca^{2+} shifted to the left compared with CON. This shift was mainly attributed to the CFs losing their stabilizing structure after undergoing heat treatment, leading to an increase in the rate of water evaporation. The second stage, spanning from 170 to 500 °C, involved the degradation of the primary structure of collagen into small peptides and amino acids. The T_d of the 0 mM Ca^{2+} group shifted to the

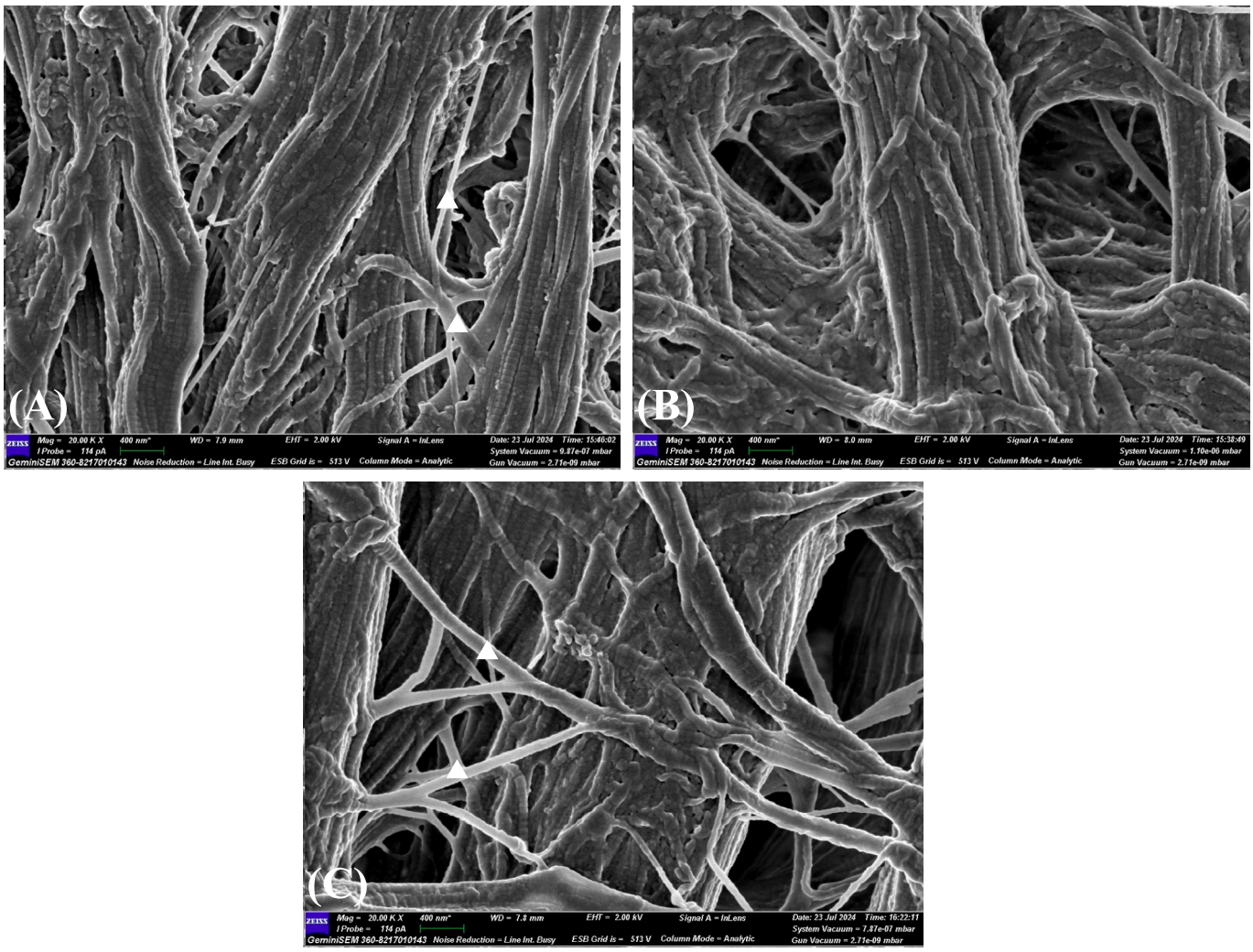

Fig. 5. Observation of microstructure in the collagen fibers(CFs) models. Scanning electron micrographs of CFs models after incubation with 0 mM Ca^{2+} (A), 5 mM Ca^{2+} (B) and 40 mM Ca^{2+} (C) by magnified ×20 k for at 37 °C for 12 h. Graph showing collagen fiber filaments (▲).

left compared with the CON. However, when a low concentration of Ca^{2+} was added, the CFs structure was preserved, leading to a gradual recovery of the T_d value. The characteristic decomposition temperatures of the 20 mM Ca^{2+} and 40 mM Ca^{2+} groups (309.61 °C and 309.51 °C, respectively) were slightly lower than that observed in the other groups (311.12 °C). This difference in decomposition temperatures indicated that high concentrations of Ca^{2+} reduced the stability of peptide bonds and promoted the degradation of CFs. This finding is consistent with the disruption of the crystal structure reported in previous sections.

3.4. Microstructure of intact fragments

The effect of different concentrations of Ca^{2+} on the microstructure of CFs is shown in Fig. 5. In the blank group, although some collagen fibers were depolymerized, the collagen fiber structure remained intact with a distinct D-band pattern(Dong et al., 2020b; Liu et al., 2018). The Ca^{2+} concentration is 5 mM, robust collagen fiber bundles with a rope-like texture were observed, consisting of parallel-arranged collagen fibrils. The addition of 40 mM Ca^{2+} led to a loose conformation of the collagen fibers, with noticeable collagen fiber filaments, which consequently reduced the structural stability of the collagen fibers.

4. Discussion

Collagen fibers primarily consist of collagen, with a small proportion of glycoproteins and proteoglycans. Under the low-temperature tenderization conditions, the group not treated with Ca^{2+} exhibited the highest dissolution of proteins and polysaccharides. XRD analysis showed that the d value in the group without Ca^{2+} increased by 0.012 nm compared with the CON group, indicating that the low-temperature conditions partially disrupted the proteoglycan bridges between collagen fibrils. Proteoglycan bridges maintain structural integrity by binding to adjacent collagen fibrils to form CFs (Puxkandl et al., 2002; Shoulders & Raines, 2009). Protein and polysaccharide dissolution decreased and then increased with an increase in Ca^{2+} concentration. This indicated that the addition of a low concentration of Ca^{2+} effectively reduced the solubility of the molecules. Although the dissolution increased with further increase in Ca^{2+} concentration, the extent of damage remained lower than that caused by low-temperature tenderization. TCA-soluble peptide levels are commonly used to evaluate the degree of degradation of all proteins (Wu et al., 2013). TCA solubility exhibited a similar trend, with higher solubility observed for the group treated with 40 mM Ca^{2+} relative to the CON group, indicating the presence of more dissolved small peptide molecules.

The shift of the amide I band and A band towards higher wavenumbers and the shift of the Amide I peak towards higher wavenumbers at 40 mM indicated a decrease in intermolecular interactions and a reduction in structural order (Liu et al., 2017). This result is consistent with previous findings on the effects of 1 mM, 7 mM, and 14 mM Ca^{2+} on collagen self-assembly (Niu et al., 2017). Collagen thermal denaturation

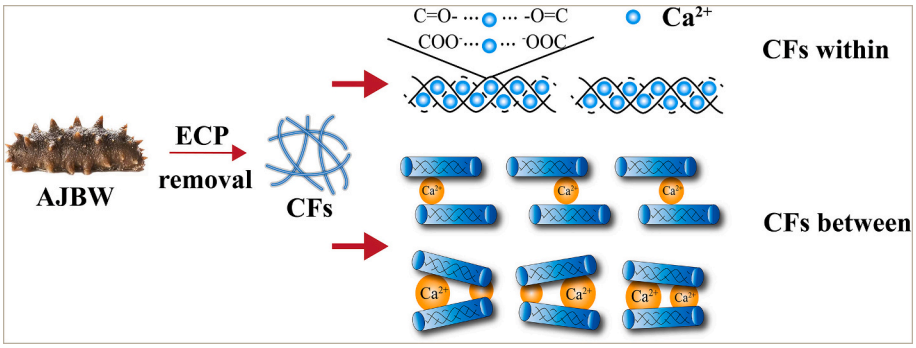

Fig. 6. Proposed mechanism for the effect of Ca^{2+} on the degree of cross-linking of CFs under low-temperature tenderization conditions.

is an irreversible process that results in unfolding of the natural triple helix structure (Makhatadze & Privalov, 1995). The results in the present study showed that the group with untreated CFs exhibited the highest stability (T_{max} = 58.41 °C), consistent with 55.79 °C reported by Liu et al., 2017. The group treated with 5 mM Ca^{2+} had the second highest stability (T_{max} = 58.211 °C), whereas the tenderized CFs had the lowest stability (T_{max} = 56.53 °C). Although the group treated with 40 mM Ca^{2+} had a lower denaturation temperature, it was still higher than the 0 mM group. TGA results showed a decrease in the characteristic decomposition temperature of CFs under high Ca^{2+} concentrations, whereas XRD analysis indicated an increased distance between CFs at 20 mM and 40 mM Ca^{2+} concentrations. These results demonstrate that low concentrations of Ca^{2+} consistently bind to CFs through hydrogen bonding and charge effects, enhancing the triple helical structure of collagen protein and improving its thermal stability. Conversely, high concentrations of Ca^{2+} infiltrate the collagen molecules and form coordination bonds with C═O groups, weakening the interactions formed by hydrogen bonding and van der Waals forces between the molecules. Consequently, the helical structures become loose or partially disintegrate, and the distances between collagen chains increase (Jia et al., 2021; Liu et al., 2023). Additionally, strong interactions between Ca^{2+} and the binding sites affect the charge stability during the self-assembly process of collagen proteins. In summary, low concentrations of Ca^{2+} promote collagen self-assembly and aid in stabilizing the collagen structure. Conversely, high concentrations of Ca^{2+} impede the self-assembly process of collagen proteins and accelerate tenderization. This conclusion is consistent with the findings reported by Niu et al., 2017.

The principal mechanism of CFs- Ca^{2+} interaction was elucidated based on these findings (Fig. 6). Ca^{2+} affects the structure and function of CFs by interacting with specific regulatory proteins. This interaction involves Ca^{2+} binding to collagenase, activating downstream signal transduction pathways, ultimately regulating the synthesis and degradation of CFs (Khan et al., 2020; Liu et al., 2019, 2017). However, this regulatory function was eliminated when CFs were isolated from AJBW and purified by removing endogenous proteinase. Additionally, Ca^{2+} is implicated in the cross-linking of CFs through interaction with other molecules. In this study, FTIR results revealed a red shift in amide A band and amide I band after the addition of Ca^{2+}, indicating the formation of coordination bonds between Ca^{2+} and the C═O group. CFs have several charged and polar groups, with carboxyl groups (-COOH) accounting for the charged groups in approximately 9.5 % of the amino acid residues (Pang et al., 2017). Carboxylic acid ionizes into $-COO^-$ form under neutral conditions. Ca^{2+} chelates $-COO^-$ to form calcium salt bridges through electrostatic interactions, resulting in a cross-linked network and enhancing the stability of CFs. When the two types of bonding reach saturation, the addition of Ca^{2+} only fills the gaps, resulting in the stretching of molecules and an increase in the intermolecular spaces. Ca^{2+} concentration that exceeds a certain threshold can adversely affect the cross-linking of CFs. Additionally, Ca^{2+} influences the structure of CFs. The presence of Ca^{2+} induces the formation of distinct structures in CFs, such as triple helical structures or other folding conformations. These structural alterations can affect the stability and mechanical properties of CFs. In this study, the DSC results revealed that CFs treated with high concentrations of Ca^{2+} exhibited lower T_{max} values. Moreover, changes in the d value of the peak A in the XRD results after the addition of Ca^{2+} indicated that Ca^{2+} modulated the triple helical structure and partially affected the self-assembly of CFs. Ca^{2+} directly binds to specific structures on collagen molecules, enhancing interactions between fiber molecules and promoting their assembly and alignment. Alternatively, Ca^{2+} can facilitate the aggregation of collagen molecules in specific spatial locations, thereby promoting the regular assembly of fibers.

5. Conclusion

In this study, acid-soluble and water-soluble components and endogenous enzymes were eliminated from AJBWs, and the intact CFs structure was retained. Subsequently, the effect of Ca^{2+} on the composition and structural stability of CFs lysate under low-temperature tenderization conditions was evaluated. Soluble proteins, polysaccharides, and small molecule peptides exhibited reduced dissolution in the groups treated with 2.5 mM and 5 mM Ca^{2+}, and increased dissolution was observed in the groups treated with 20 mM and 40 mM Ca^{2+}, compared to the group without Ca^{2+}. FTIR, DSC, TGA, and XRD analyses showed that high concentration of Ca^{2+} caused a decrease in crystallinity and weakening of the interactions across the three chains of collagen. These changes increased the distance between the molecular chains and led to a decrease in thermal stability. Conversely, low concentrations of Ca^{2+} exhibited a protective effect, promoting the self-assembly of CFs. These results provide a theoretical reference for elucidating the effect of Ca^{2+} on the CFs structure of sea cucumber and a basis for enhancing the quality of sea cucumber through low-temperature tenderization.

CRediT authorship contribution statement

Chen Zhang: Writing – original draft, Methodology, Formal analysis, Data curation, Conceptualization. **Wei Wang:** Visualization, Investigation. **Hongyan Li:** Investigation, Data curation. **Hongxia Che:** Methodology, Formal analysis. **Wancui Xie:** Resources, Funding acquisition. **Wenming Ju:** Validation, Software. **Hang Qi:** Visualization, Supervision. **Xiufang Dong:** Supervision, Project administration, Funding acquisition, Conceptualization.

Declaration of competing interest

The authors declare that they have no known competing financial interests or personal relationships that could have appeared to influence the work reported in this paper.

Acknowledgements

This work was supported by Natural Science Foundation of Shandong Province (ZR2021QC168), Science and Technology-Driven Small and Medium-sized Enterprises Innovation Capacity Enhancement Project of Shandong Province (2023TSGC0766, 2021TSGC1251, 2023TSGC0389) and Special Funds for Centralized Guidance of Local Development Project (YDZX2022176).

Data availability

Data will be made available on request.

References

Bu, H. H., Yang, H., Shen, L. R., Liu, W. T., & Li, G. Y. (2020). Glutamic acid concentration dependent collagen mineralization in aqueous solution. *Colloids And Surfaces. B: Biointerfaces, 190*, Article 110892. https://doi.org/10.1016/j.colsurfb.2020.110892

Dong, X. F., He, B. Y., Jiang, D., Yu, C. X., Zhu, B. W., & Qi, H. (2020). Proteome analysis reveals the important roles of protease during tenderization of sea cucumber *Apostichopusjaponicus* using iTRAQ. *Food Research International, 131*, Article 108632. https://doi.org/10.1016/j.foodres.2019.108632

Dong, X. F., Qi, H., Feng, D. D., He, B. Y., Nakamura, Y., Yu, C. X., & Zhu, B. W. (2018). Oxidative stress involved in textural changes of sea cucumber *Stichopus japonicus* body wall during low-temperature treatment. *International Journal of Food Properties, 21*(1), 2646–2659. https://doi.org/10.1080/10942912.2018.1559187

Dong, X. F., Shen, P., Yu, M. Q., Yu, C. X., Zhu, B. W., & Qi, H. (2020). (−)-epigallocatechin gallate protected molecular structure of collagen fibers in sea cucumber *Apostichopus japonicus* body wall during thermal treatment. *LWT-Food Science and Technology, 123*, Article 109076. https://doi.org/10.1016/j.lwt.2020.109076

Dong, X. F., Yang, X. H., Li, H. Y., Che, H. X., Song, L., Chen, X., … H.. (2021). Effects of oxidation on the structure of collagen fibers of sea cucumber (*Apostichopus japonicus*) body wall during thermal processing. *LWT-Food Science and Technology, 138*, Article 110528. https://doi.org/10.1016/j.lwt.2020.110528

DuBois, M., Gilles, K. A., Hamilton, J. K., Rebers, P. T., & Smith, F. (1956). Colorimetric method for determination of sugars and related substances. *Analytical Chemistry, 28*(3), 350–356. https://doi.org/10.1021/ac60111a017

Gao, D. G., Cheng, Y. M., Wang, P. P., Li, F., Wu, Y. K., Lyu, B., … J. B.. (2020). An eco-friendly approach for leather manufacture based on P (POSS-MAA)-aluminum tanning agent combination tannage. *Journal of Cleaner Production, 257*, Article 120546. https://doi.org/10.1016/j.jclepro.2020.120546

Ge, X. T., Wang, H. L., Yin, M. Y., & Wang, X. C. (2022). Effect of different thawing methods on the physicochemical properties and microstructure of frozen instant sea cucumber. *Foods, 11*(17), 2616. https://doi.org/10.3390/foods11172616

Guo, Y. C., Ming, Y., Li, X., Sun, C. H., Dong, X. P., & Qi, H. (2024). Effect of phlorotannin extracts from Ascophyllum nodosum on the textural properties and structural changes of Apostichopus japonicus. *Food Chemistry, 437*, Article 137918. https://doi.org/10.1016/j.foodchem.2023.137918

He, X. F., Xie, L. L., Zhang, X. S., Lin, F., Wen, X. B., & Teng, B. (2021). The structural characteristics of collagen in swim bladders with 25-year sequence aging: The impact of age. *Applied Sciences, 11*(10), 4578. https://doi.org/10.3390/app11104578

Jia, D., You, J., Hu, Y., Liu, R., & Xiong, S. B. (2015). Effect of $CaCl_2$ on denaturation and aggregation of silver carp myosin during setting. *Food Chemistry, 185*, 212–218. https://doi.org/10.1016/j.foodchem.2015.03.130

Jia, W., Shi, Q. Y., Zhang, R., Shi, L., & Chu, X. G. (2021). Unraveling proteome changes of irradiated goat meat and its relationship to off-flavor analyzed by high-throughput proteomics analysis. *Food Chemistry, 337*, Article 127806. https://doi.org/10.1016/j.foodchem.2020.127806

Khan, M., Liu, H. L., Wang, J., & Sun, B. G. (2020). Inhibitory effect of phenolic compounds and plant extracts on the formation of advance glycation end products: A comprehensive review. *Food Research International, 130*, Article 108933. https://doi.org/10.1016/j.foodres.2019.108933

Laemmli, U. K. (1970). Cleavage of structural proteins during the assembly of the head of bacteriophage T4. *Nature, 227*(5259), 680–685. https://doi.org/10.1038/227680a0

Li, X., Sun, Y. Y., Pan, D. D., Wang, Y., & Cao, J. X. (2017). The effect of $CaCl_2$ marination on the tenderizing pathway of goose meat during conditioning. *Food Research International, 102*, 487–492. https://doi.org/10.1016/j.foodres.2017.09.014

Li, Y. Y., Qi, X., Fan, C. Z., Fan, Y., Zhang, H. W., Zhang, J. J., & Hou, H. (2024). Novel synergistic cross-linking ameliorate ready-to-eat sea cucumber deterioration and its quantum chemical analysis. *Food Chemistry, 439*, Article 138097. https://doi.org/10.1016/j.foodchem.2023.138097

Liu, F., Yu, Z., Wang, B. B., & Chiou, B. S. (2023). Changes in structures and properties of collagen fibers during collagen casing film manufacturing. *Foods, 12*(9), 1847. https://doi.org/10.3390/foods12091847

Liu, Y. X., Liu, Z. Q., Song, L., Ma, Q. R., Zhou, D. Y., Zhu, B. W., & Shahidi, F. (2019). Effects of collagenase type I on the structural features of collagen fibres from sea cucumber (*Stichopus japonicus*) body wall. *Food Chemistry, 301*, Article 125302. https://doi.org/10.1016/j. foodchem.2019.125302

Liu, Y. X., Zhou, D. Y., Ma, D. D., Liu, Y. F., Li, D. M., Dong, X. P., … B. W.. (2016). Changesin collagenous tissue microstructures and distributions of cathepsin L in body wall of autolytic sea cucumber (*Stichopus japonicus*). *Food Chemistry, 212*, 341–348. https://doi.org/10.1016/j.foodchem.2016.05.173

Liu, Y. X., Zhou, D. Y., Ma, D. D., Liu, Z. Q., Liu, Y. F., Song, L., … F.. (2017). Effects of endogenous cysteine proteinases on structures of collagen fibres from dermis of sea cucumber (*Stichopus japonicus*). *Food Chemistry, 232*, 10–18. https://doi.org/10.1016/j.foodchem.2017.03.155

Liu, Z. Q., Tuo, F. Y., Song, L., Liu, Y. X., Dong, X. P., Li, D. L., & Shahidi, F. (2018). Action of trypsin on structural changes of collagen fibres from sea cucumber (*Stichopus japonicus*). *Food Chemistry, 256*, 113–118. https://doi.org/10.1016/j.foodchem.2018.02.117

Makhatadze, G. I., & Privalov, P. L. (1995). Energetics of protein structure. *Advances in Protein Chemistry, 43*, 307–425. https://doi.org/10.1016/S0065-3233(08)60548-3

Niu, X. F., Fan, R., Tian, F., Guo, X. L., Li, P., Feng, Q. L., & Fan, Y. B. (2017). Calcium concentration dependent collagen mineralization. *Materials Science and Engineering: C, 73*, 137–143. https://doi.org/10.1016/j.msec.2016.12.079

Pang, X. C., Lin, L. J., & Tang, B. (2017). Unraveling the role of calcium ions in the mechanical properties of individual collagen fibrils. *Scientific Reports, 7*(1), 46042. https://doi.org/10.1038/srep46042

Puxkandl, R., Zizak, I., Paris, O., Keckes, J., Tesch, W., Bernstorff, S., & Fratzl, P. (2002). Viscoelastic properties of collagen: Synchrotron radiation investigations and structural model. *Philosophical Transactions of the Royal Society of London. Series B: Biological Sciences, 357*(1418), 191–197. https://doi.org/10.1098/rstb.2001.1033

Shakouri, A., Nabavi, M. B., Kochanian, P., Savari, A., Safahieh, A., & Aminrad, T. (2009). New observation of two species of sea cucumbers from Chabahar Bay (southeast coasts of Iran). *Asian Joural of Animal Sciences, 3*(4), 130–134. https://doi.org/10.3923/ajas.2009.130.134

Shoulders, M. D., & Raines, R. T. (2009). Collagen structure and stability. *Annual Review of Biochemistry, 78*, 929–958. https://doi.org/10.1146/annurev.biochem.77.032207.120833

Song, X., Si, L. L., Sun, X., Zhu, X., Li, Z. X., Li, Y. Y., … H.. (2022). Rheological properties,thermal stability and conformational changes of collagen from sea cucumber (*Apostichopus japonicas*). *Food Chemistry, 389*, Article 133033. https://doi.org/10.1016/j.foodchem.2022.133033

Thongchai, K., Chuysinuan, P., Thanyacharoen, T., Techasakul, S., & Ummartyotin, S. (2020). Characterization, release, and antioxidant activity of caffeic acid-loaded collagen and chitosan hydrogel composites. *Journal of Materials Research and Technology, 9*(3), 6512–6520. https://doi.org/10.1016/j.jmrt.2020.04.036

Thurmond, F. A., & Trotter, J. A. (1996). Morphology and biomechanics of the microfibrillar network of sea cucumber dermis. *Journal of Experimental Biology, 199*(8), 1817–1828. https://doi.org/10.1242/jeb.199.8.1817

Tian, M., Xue, C. H., Chang, Y. G., Shen, J. J., Zhang, Y. Y., Li, Z. J., & Wang, Y. C. (2020). Collagen fibrils of sea cucumber (*Apostichopus japonicus*) are heterotypic. *Food Chemistry, 316*, Article 126272. https://doi.org/10.1016/j.foodchem.2020.126272

Wang, Y., Zhou, Y., Wang, X. X., Ma, F., Xu, B. C., Li, P. J., & Chen, C. G. (2020). Origin of high-pressure induced changes in the properties of reduced-sodium chicken myofibrillar proteingels containing $CaCl_2$: Physicochemical and molecular modification perspectives. *Food Chemistry, 319*, Article 126535. https://doi.org/10.1016/j.lwt.2020.109461

Wu, H. T., Li, D. M., Zhu, B. W., Sun, J. J., Zheng, J., Wang, F. L., … X.. (2013). Proteolysis of noncollagenous proteins in sea cucumber, *Stichopus japonicus*, body wall: Characterisation and the effects of cysteine protease inhibitors. *Food Chemistry, 141*(2), 1287–1294. https://doi.org/10.1016/j.foodchem.2013.03.088

Xu, Z. J., Yang, Y., Zhao, W. L., Wang, Z. Q., Landis, W. J., Cui, Q. Q., & Sahai, N. (2015). Molecular mechanisms for intrafibrillar collagen mineralization in skeletal tissues. *Biomaterials, 39*, 59–66. https://doi.org/10.1016/j.biomaterials.2014.10.048

Yan, X. Y., Chen, Y. N., Dan, N. H., & Dan, W. H. (2022). A novel thermosensitive growth-promoting collagen fibers composite hemostatic gel. *Journal of Materials Chemistry B, 10*(21), 4070–4082. https://doi.org/10.1039/D1TB02644E

Yang, J. F., Gao, R. C., Wu, H. T., Li, P. F., Hu, X. S., Zhou, D. Y., & Su, Y. C. (2015). Analysis of apoptosis in ultraviolet-induced sea cucumber (*Stichopus japonicus*) melting using terminal deoxynucleotidyl-transferase-mediated dUTP nick end-labeling assay and cleaved caspase-3 immunohistochemistry. *Journal of Agricultural and Food Chemistry, 63*(43), 9601–9608. https://doi.org/10.1021/acs.jafc.5b03453

Yu, X. L., Guo, L. F., Liu, M., Cao, X. S., Shang, S., Liu, Z. X., … L. B.. (2018). Callicarpa nudiflora loaded on chitosan-collagen/organomontmorillonite composite membrane for antibacterial activity of wound dressing. *International Journal of Biological Macromolecules, 120*, 2279–2284. https://doi.org/10.1016/j.ijbiomac.2018.08.113

Zheng, X., Chen, Y. N., Dan, N. H., Li, Z. J., & Dan, W. H. (2022). Anti-calcification potential of collagen based biological patch crosslinked by epoxidized polysaccharide. *International Journal of Biological Macromolecules, 209*, 1695–1702. https://doi.org/10.1016/j.ijbiomac.2022.04.117

Zhou, Y. G., & Yang, H. S. (2019). Effects of calcium ion on gel properties and gelation of tilapia (Oreochromis niloticus) protein isolates processed with pH shift method. *Food Chemistry, 277*, 327–335. https://doi.org/10.1016/j.foodchem.2018.10.110

Zou, Y., Wang, L. J., Niu, Y. W., Song, S. Q., Yang, B., Qin, X. J., … D. Y.. (2023). The effect on product structure and volatile compounds of chicken liver by fermentation. *LWT-Food Science and Technology, 189*, Article 115515. https://doi.org/10.1016/j.lwt.2023.115515